Supporting Information: The Substrate-Bound Crystal Structure of a Baeyer–Villiger Monooxygenase Exhibits a Criegee-like Conformation

Brahm J. Yachnin,[†,⊥] Tara Sprules,[#] Michelle B. McEvoy,[†] Peter C. K. Lau,[‡,§,∥] Albert M. Berghuis*[,†,‡,⊥]

Departments of [†]Biochemistry, [‡]Microbiology & Immunology, and [§]Chemistry, McGill University, 3649 Promenade Sir William Osler, Bellini Pavilion, Room 466, Montreal, QC, Canada, H3G 0B1

[∥]Biotechnology Research Institute, National Research Council of Canada, 6100 Royalmount Ave., Montreal, QC, Canada H4P 2R2

[#]Québec/Eastern Canada High Field NMR Facility, 3420 University St., Room 023, Montreal, QC, Canada, H3A 2A7

[⊥]Groupes de recherche GRASP et PROTEO, Canada.

EXPERIMENTAL SECTION

Subcloning the *chnB1* gene into the pJW234 expression vector

The *chnB1* gene was amplified using *Pwo* DNA polymerase (Roche) from the pSDRmchnB1 plasmid.[1] PCR primers with *Nsi*I and *Eco*RI restriction sites were used to amplify the gene (restriction sites are underlined), as shown in Table S2. The desired band was purified using the QIAquick Gel Extraction Kit (Qiagen) and subcloned into the pPCR-Script Cam vector (Stratagene) using the PCR-Script Cam Cloning Kit (Stratagene). Plasmid DNA from positive clones was prepared using the QIAprep Spin MiniPrep kit (Qiagen), and then digested using *Nsi*I and *Eco*RI (New England BioLabs). The pJW234 expression vector (obtained from Dr. Mirek Cygler, University Saskatchewan, Saskatoon, Canada) was digested with the same enzymes. The desired bands from both digests were purified using gel extraction (MO BIO Laboratories UltraClean 15 DNA Purification Kit). The *chnB1* insert was ligated into the pJW234 vector, and this plasmid was used to transform *E. coli* DH5α cells. Plasmid DNA from positive clones was prepared using the QIAprep Spin MiniPrep kit (Qiagen), and DNA sequencing was used to confirm the sequence (McGill University and Genome Quebec Innovation Centre Sequencing Service, Montreal, Canada). The resultant plasmid is called His_8-TEV-ChnB1.

Creation of the L145N, L145D, and F507Y Mutants

The His_8-TEV-ChnB1 plasmid was amplified using the protocol from the Agilent QuikChange II Site-Directed Mutagenesis Kit. The primers used are shown in Table S2, with the altered bases underlined. Plasmid DNA from positive clones was prepared and sequenced as described above.

Expression and Purification of CHMO

The expression and purification protocols for wild-type CHMO and its mutants are identical. *E. coli* Rosetta(DE3) (Novagen) cells were transformed with His_8-TEV-ChnB1 plasmid and the strain was grown in 50 mL of LB supplemented with 100 μg/mL of ampicillin and 30 μg/mL of chloramphenicol and grown for 16-18 hours at 37°C. This was then subcultured into a fresh 50 mL culture and grown for an additional 6 hours. After another subculturing in fresh 1 L culture and growth at 37°C to an OD_{600} of 0.5-0.6, the cells were induced with 1 mM IPTG and allowed to grow at 15°C for 18-20 hours.

All subsequent steps were performed at 4°C. The cells were harvested using centrifugation (6000×g for 10 minutes). The pellets were resuspended in 50 mM sodium phosphate, 0.3 M sodium chloride, 10 mM imidazole, pH 8.0, and a Complete Mini (EDTA-free) protease inhibitor tablet (Roche) was added. The cells were lysed by sonication, and the crude extract was clarified using centrifugation (21,000×g for 30-60 minutes). The lysate was then filtered. Purification procedures were performed on an Akta Explorer (GE Healthcare). The lysate was loaded onto a 5 mL Ni-NTA Superflow Cartridge (Qiagen) equilibrated with 50 mM sodium phosphate, 0.3 M sodium chloride, 10 mM imidazole, pH 8.0. The protein was eluted using a linear gradient to 50 mM sodium phosphate, 0.3 M sodium chloride, 300 mM imidazole, pH 8.0. Fractions containing CHMO were pooled. For samples to be used for enzyme kinetics or NMR, the protein was dialysed against 50 mM sodium phosphate pH 8.0 and then concentrated to approximately 30 mg/mL. For samples to be used for crystallization, the pooled sample was digested using His-tagged tobacco etch virus (TEV) protease S219V (purified in house, plasmid obtained from Dr. Mirek Cygler) while dialysing the sample against 50 mM sodium phosphate, 150 mM sodium chloride, 5 mM sodium citrate, 1 mM DTT, pH 8.0 overnight. The sample was then re-loaded onto the Ni-NTA column to remove undigested CHMO and the TEV protease. The unbound protein was pooled and concentrated (Millipore Centriprep concentrators) to about 5 mL. The sample was supplemented with FAD and allowed to stand for about 4 hours. The sample was then loaded onto a HiLoad Superdex 75 26/60 prep grade column (GE Healthcare) equilibrated with 50 mM sodium phosphate, 150 mM sodium chloride, pH 8.0. Fractions containing CHMO were pooled and concentrated. Purity was assessed using SDS-PAGE throughout the purification. The buffer was exchanged to 50 mM Tris pH 8.0 by running the sample on a PD-10 desalting column (GE Healthcare). The sample was concentrated to 5 mg/mL and supplemented with a 5-fold molar excess of FAD and $NADP^+$.

Saturation Transfer Difference NMR Spectroscopy

Basic information regarding the STD NMR experiments is provided in the main article. Additional information is provided here. The irradiation power was $(\gamma/2\pi)B_1$= 80 Hz applied through a train of 50 ms gaussian pulses with a 100 μs delay between the pulses. Experiments were recorded with saturation times of 2 s. The relaxation delay was set to 3 s. A 30 ms spin-lock pulse with a strength of $(\gamma/2\pi)B_1$= 3000 Hz was used to eliminate background protein signals. Spectra were recorded with 32k points, a sweep width of 16 ppm, and 128 transients. The experiments were repeated the next day in order to ensure that the samples were stable. The intensity of each peak in the STD spectrum was divided by the intensity in the reference spectrum. In order to determine the percent STD effect, this ratio was divided by the same ratio for

the largest peak in the STD spectra, the A2 proton of the adenine ring. In those cases where multiplets were observed for a single proton, the percent STD effect was averaged for each peak in the multiplet. The data from the two replicates were averaged to obtain a final value for each proton.

RESULTS

The following figures and table are described in the text of main article.

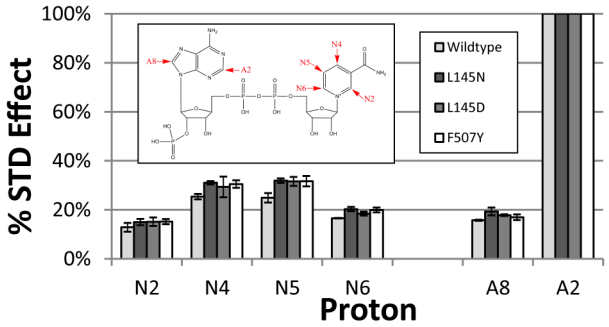

Figure S1. The percent STD effect for the nicotinamide (left) and adenine (right) protons, using A2 as a reference, for the wild-type and the three mutant enzymes. Error bars show the standard deviation. The structure of NADP$^+$ is shown inset, with the positions of each proton indicated.

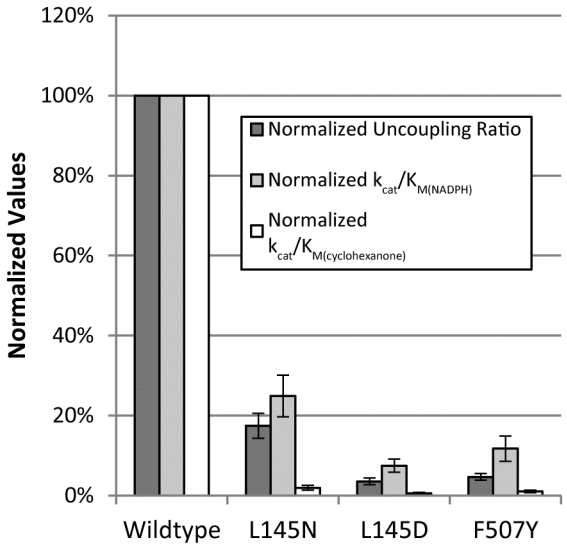

Figure S2. The uncoupling ratio is compared to $k_{cat}/K_{M(NADPH)}$ and $k_{cat}/K_{M(cyclohexanone)}$. All values are normalized to the corresponding wild-type values. Error bars indicate the standard deviations for each value. The standard deviation of the wild-type uncoupling ratio is included in the k_{cat}/K_M error bars in order to account for error in scaling k_{cat}/K_M values to the wild-type uncoupling ratio.

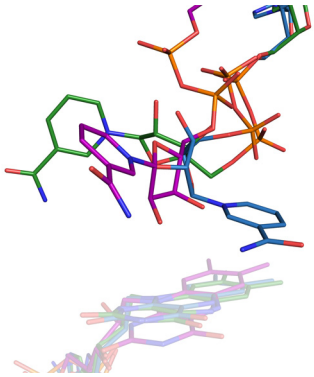

Figure S3. The NADP$^+$ conformations in the $CHMO_{Closed}$ (blue) and $CHMO_{Rotated}$ (green) structures are compared to the rotated NADP$^+$ conformation of *m*FMO (purple, PDB ID 2XLR). The structures were superimposed using the FAD molecule, which is also shown.

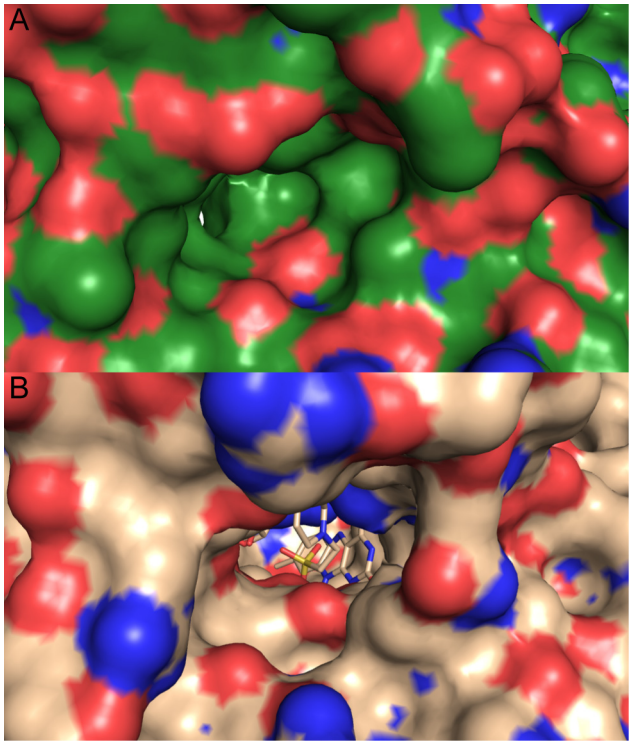

Figure S4. Comparison of the "back" of CHMO (panel A, green, $CHMO_{Rotated}$ conformation) and PAMO (panel B, wheat, PDB ID 2YLT). The protein is shown as a surface, and the ligands (FAD, NADP$^+$, cyclohexanone, and MES) are shown as sticks. The large tunnel seen in PAMO is obstructed in CHMO, obscuring the view of the FAD, NADP$^+$, and cyclohexanone in the CHMO structure.

Table S1. Enzyme kinetics data. Errors are the standard errors determined by regression, or standard deviations for the Uncoupling Ratio.

		Wild-type	L145N	L145D	F507Y
K_M (M)	NADPH	(6.19±0.70) × 10^{-6}	(3.53±0.34) × 10^{-6}	(4.46±0.47) × 10^{-6}	(3.34±0.63) × 10^{-6}
	Cyclo-hexanone	(2.95±0.72) × 10^{-7}	(2.46±0.26) × 10^{-6}	(4.93±1.95) × 10^{-7}	(1.14±0.11) × 10^{-6}
k_{cat} (s^{-1})	NADPH	12.47±0.47	1.77±0.05	0.67±0.02	0.79±0.04
	Cyclo-hexanone	8.86±0.47	1.45±0.05	0.080±0.004	0.36±0.01
k_{cat}/K_M ($M^{-1}s^{-1}$)	NADPH	(2.01±0.24) × 10^6	(5.02±0.51) × 10^5	(1.51±0.17) × 10^5	(2.37±0.46) × 10^5
	Cyclo-hexanone	(3.00±0.75) × 10^7	(5.89±0.66) × 10^5	(1.63±0.65) × 10^5	(3.16±0.31) × 10^5
Uncoupling Ratio		114±16	20±2	4±1	5±1
K_i (M)	$NADP^+$	(1.65±0.19) × 10^{-4}	(4.20±0.75) × 10^{-5}	N.D. ($<10^{-4}$)	(1.92±0.38) × 10^{-4}

Inhibition of CHMO and Mutants by $NADP^+$

In order to estimate the affinity of $NADP^+$, the K_i vaules of the wild-type and the mutants were determined using $NADP^+$ as the inhibitor and varying NADPH as the substrate (Table S1). As expected, $NADP^+$ appeared to behave as a competitive inhibitor for CHMO. $NADP^+$ proved to be only a weak inhibitor of *Rm*CHMO, in contrast to *Ac*CHMO[2] and PAMO,[3] which have K_i values in the low micromolar range, but similar to 4-hydroxyacetophenone monooxygenase (HAPMO).[4] In comparison to the *Rm*CHMO wild-type enzyme, the L145N mutant is more sensitive to inhibition by $NADP^+$. The L145D mutant also shows this same trend, but an accurate K_i could not be determined due to the low activity of this mutant. The F507Y mutant reveals that it is similar to the wild-type enzyme, in this respect.

The $NADP^+$ inhibition studies imply that the affinity of $NADP^+$ is much weaker than would have been suggested by the values for $K_{M(NADPH)}$; however, as $NADP^+$ is known to stay bound to the enzyme throughout the catalytic mechanism (see Figure 5), and readily co-crystallizes with *Rm*CHMO, it must be concluded that this apparent weak affinity is at least partially caused by complex binding kinetics. Despite this puzzling aspect, the mutants display K_i values that are less or statistically equal to that of the wild-type enzyme, mirroring the trend in affinity seen by monitoring $K_{M(NADPH)}$.

DISCUSSION

As described in the main article, the uncoupling ratio data are consistent with the interpretation that the mutants are less effective in stabilizing the peroxyanion intermediate than the wild-type enzyme. The uncoupling ratio represents the ratio between the enzyme catalyzing the full BV reaction (BV activity), and a short-circuited reaction in which NADPH is merely oxidized (NAPDH oxidase activity). In the wild-type enzyme, the full BV reaction is dramatically favored, as indicated by a ratio of 114. The three mutants are all less efficient in favoring the BV reaction, as shown with their uncoupling ratios of 20 or less. This implies that the mutants are either defective in catalyzing the full BV reaction, enhanced in the short-circuited NADPH oxidation reaction, or both. The steady-state kinetics data indicate that the mutants do have compromised BV activity. To access whether the mutations also enhanced NADPH oxidase activity, we compared both the normalized $k_{cat}/K_{M(NADPH)}$ and the normalized $k_{cat}/K_{M(cyclohexanone)}$ to the normalized uncoupling ratio (with wild-type values set to 100%). This analysis provides insights into how efficiently each substrate is used by the enzymes (see Figure S2). Of course, the mutants are less efficient catalysts both with respect to NADPH and cyclohexane. Intriguingly, using the drop in uncoupling ratios as a base for the extent of anticipated efficiency loss, the mutants are actually using NADPH more effectively than predicted. Conversely, the mutants use cyclohexanone as a substrate much less efficiently than would be anticipated. This observation implies that the mutations have differential impact on the BV and NADPH oxidase reactions. Given that the only unique step in the NADPH oxidase pathway, as compared to the BV activity pathway, is the unproductive collapse of the peroxyanion intermediate without formation of the Criegee intermediate, we conclude that the mutants destabilize this peroxyanion intermediate. In so doing, the peroxyanion intermediate is more likely to collapse unproductively prior to the arrival of the ketone substrate. The $CHMO_{Rotated}$ crystal structure readily rationalizes this property of the mutants. In contrast to the Closed conformation, $NADP^+$ cannot play a role in stabilizing the peroxyanion intermediate in the Rotated conformation.

REFERENCES

(1) Mirza, I. A.; Yachnin, B. J.; Wang, S.; Grosse, S.; Bergeron, H.; Imura, A.; Iwaki, H.; Hasegawa, Y.; Lau, P. C. K.; Berghuis, A. M. *J. Am. Chem. Soc.* **2009**, *131*, 8848.

(2) Sheng, D.; Ballou, D. P.; Massey, V. *Biochemistry* **2001**, *40*, 11156.

(3) Torres Pazmiño, D. E.; Baas, B.-J.; Janssen, D. B.; Fraaije, M. W. *Biochemistry* **2008**, *47*, 4082.

(4) van den Heuvel, R. H. H.; Tahallah, N.; Kamerbeek, N. M.; Fraaije, M. W.; van Berkel, W. J. H.; Janssen, D. B.; Heck, A. J. R. *J. Biol. Chem.* **2005**, *280*, 32115.

Table S2. PCR primers for subcloning and site-directed mutagenesis. Restriction sites are double underlined and mutated bases are single underlined.

Construct	Primer	Sequence
His_8-TEV-ChnB1	Sense	5'-CAGGAAACAATGCATATGACCGCACAG-3'
His_8-TEV-ChnB1	Antisense	5'-CAGTACAGAATTCTCAGACCGTGACCATCTC-3'
His_8-TEV-ChnB1-L145N	Sense	5'-GTCGTCAACGCCGTGGGCAATCTCTCCGCGATCAACTTC-3'
His_8-TEV-ChnB1-L145N	Antisense	5'-GAAGTTGATCGCGGAGAGATTGCCCACGGCGTTGACGAC-3'
His_8-TEV-ChnB1-L145D	Sense	5'-GTCGTCAACGCCGTGGGAGATCTCTCCGCGATCAACTTC-3'
His_8-TEV-ChnB1-L145D	Antisense	5'-GAAGTTGATCGCGGAGAGATCTCCCACGGCGTTGACGAC-3'
His_8-TEV-ChnB1-F507Y	Sense	5'-GCCGAGCGTACTGTATTACCTGGGCGGCCTG-3'
His_8-TEV-ChnB1-F507Y	Antisense	5'-CAGGCCGCCCAGGTAATACAGTACGCTCGGC-3'